Predicting extremes: influenza epidemics in France

Maud Thomas, Holger Rootzén

Predicting extremes: influenza epidemics in France

Maud Thomas and Holger Rootzén

October 23, 2019

Abstract

Influenza epidemics each year cause hundreds of thousands of deaths worldwide and put high loads on health care systems, in France and elsewhere. A main concern for resource planning in public health is the risk of an extreme and dangerous epidemic. Sizes of epidemics are measured by the number of visits to doctors caused by Influenza Like Illness (ILI), and health care planning relies on prediction of ILI rates. We use recent results on the multivariate Generalized Pareto (GP) distributions in Extreme Value Statistics to develop methods for real-time prediction of risks of exceeding very high levels and for detection of unusual and potentially very dangerous epidemics. Based on the observation of the two first weeks of the epidemic, the GP method for real-time prediction is employed to predict ILI rates of the third week and the total size of the epidemic for extreme influenza epidemics in France. We then apply a general anomaly detection framework to the ILI rates during the three first weeks of the epidemic for early detection of unusual extreme epidemics. As an additional input to resource planning we use standard methods from extreme value statistics to estimate risk of exceedance of high ILI levels in future years. The new methods are expected to be broadly applicable in health care planning and in many other areas of science and technology.

1 Introduction

Influenza every year causes 250,000–500,000 deaths worldwide [Rambaut et al., 2008] and 0–10,000 deaths in France [Viboud et al., 2004]. In the 20th century there were 3 influenza pandemics, with the very extreme and unusual 1918 Spanish flu causing perhaps 50 million deaths [Simonsen et al., 1998]. Annual seasonal influenza epidemics put substantial strain on public health care systems, in France because the high morbidity leads to emergency rooms becoming overfilled, and also by the work caused by excess deaths. Countrywide data on morbidity is typically available in the form of counts of visits to doctors caused by Influenza Like Illness (ILI).

Substantial epidemiological research is aimed at the impact of annual seasonal influenza epidemics on the health care system. Key problems include

(P1) estimation of risks of very extreme ILI rates next year — or during the next 10 years,

(P2) real-time prediction of risks of high ILI rates in extreme epidemics, and

(P3) detection of anomalous and unusual, potentially very dangerous, extreme epidemics.

These three key problems concern prediction outside of the range of observed data. Extreme value statistics (EVS) is the branch of statistics which has been developed to address problems like the ones raised above, and to extrapolate outside the range of data. It is broadly used to handle extreme events, such as extreme floods or heat waves or episodes with huge financial losses [Katz et al., 2002, Embrechts et al., 1997]. In this paper we build on recently developed EVS results on multivariate Generalized Pareto (GP) distributions to extend the toolbox of available epidemiological techniques, by using them to give consistent answers to Problems (P1), (P2) and (P3). We then use the new tools for prediction of the ILI rates during the third week and of the total size for influenza epidemics in France, and for evaluating the risk that a new epidemic is anomalous. The methods we have developed in this paper can be used more broadly, e.g. for prediction of extremes of other types of recurrent community epidemics or for dimensioning of capabilities to handle health problems caused by extreme heat waves.

A central issue for resource planning in public health is to predict the likelihood that exceptional or extreme courses of events occur in the not too distant future [Bresee and Hayden, 2013]. We use ILI data from France, collected by the Sentinelles network [Réseau Sentinelles, 2019]. In this data a visit to a doctor is classified as ILI using the following three criteria, i) fever in excess of 39 degrees centigrades, ii) respiratory symptoms, and iii) muscle aches. Only a part of the ILI cases are actually caused by influenza, but of course the total number measures the burden on the health care system. There is an influenza epidemic in France each year, and the estimated yearly peak number of ILI visits to health care providers during a week varies between 200,000 and 900,000, cf. Figure 1 below.

Problem (P1) is solved by standard and well established methods from EVS. As for previous use in epidemiology, we only know of two papers: in 2015, Chen et al. applied EVS to monthly incidence of avian influenza cases, and in 2016, Thomas et al. illustrated the use of EVS to estimate distributions of extremes of annual seasonal influenza mortality and variations by weekday in the daily number of emergency department visits. As far as we understand, classical SIR modeling is not suitable for the large influenza epidemics where sizes of outbursts are determined by macro scale events such as high genetic variability and frequent genetic reassortment of viruses, and substantial variation in efficiencies of vaccines and in vaccination frequency [Rambaut et al., 2008].

Previous approaches to Problem (P2) include high dimensional times series prediction [Davis et al., 2016]. The Sentinelles network uses a nonparametric "nearest neighbor" method to predict the evolution of the epidemic. The US Center for Disease Control initiated a data challenge to predict the year 2013 US influenza epidemic. Their conclusion was "Forecasting has become technically feasible, but further efforts are needed to improve forecast accuracy so that policy makers can reliably use these predictions" [Biggerstaff et al., 2016].

Solutions to Problem (P3) can be seen as a warning systems for early managing of unusual and potentially dangerous extreme epidemics. We are aware of two previous papers that used EVS in the context of surveillance: Guillou and Kratz [2013] proposed a method for early detection of time clusters applied to the surveillance of Salmonella and Thomas et al. [2017] presented an anomaly detection algorithm in extreme regions using empirical Minimum-Volume sets on the sphere.

The approach in the present paper, built on a Generalized Pareto likelihood, can add corroboration or otherwise to fears that an anomalous event occurs.

A problem which is important for health care planning is to decide when the yearly influenza epidemic has started. Papers studying this question include [Le Strat and Carrat, 1999] which proposes an automatic detection method based on hidden Markov models. The Sentinelles network uses the "Serfling method" [Serfling, 1963] which is built on cyclical seasonal modeling of background ILI rates and pronounces that the annual influenza epidemic has started when ILI rates during two consecutive weeks exceeds the upper bound of the 90% confidence interval for the weekly seasonal mean. Here we propose a third method, adapted to our problem, to define the start of an influenza epidemic.

The next section gives a very brief account of the Peaks over Threshold (PoT) method in EVS. Section 3 describes the ILI data in more detail and how we select the extreme part of epidemics. Section 4 presents the methods we use and in particular the multivariate GP distributions which form the basis for the approach to Problems (P2) and (P3) which is developed in this paper. The section also discusses the GP likelihood approach for measuring anomalous character of a new epidemic which can contribute to solutions of Problem (P3). In Section 5 the EVS methods are applied to the Sentinelles ILI data and Section 6 studies the accuracy of the real-time prediction, based on Brier plots and scores. Finally, Section 7 contains a concluding discussion.

2 Background: EVS modeling

EVS builds on two methods, the block maxima method which applies to, say, yearly maxima of some quantity of interest, and the Peaks over Thresholds (PoT) method, which is the one we will use here.

The approach to Problem (P1) is based on the one-dimensional version of the PoT method in which one defines a suitably high threshold and only uses the excesses (= observation − threshold) as the data for the statistical analysis. E.g. the observations could be the ILI rates of the third week of an influenza epidemic and the data to be analyzed could be the excesses of the 0.3 quantile of these rates. In the statistical analysis these excesses, given that they are positive, are then assumed to be independent and identically distributed and to follow a GP distribution, and the parameters of this GP distribution are estimated from the data. The estimated distribution can then, e.g., be used to compute risks that there will be a very high ILI rate next year, or during the next 10 years. A useful account of this method is given in [Coles, 2001].

The multivariate PoT method, basis for the approach to Problems (P2) and (P3), is much more recent. In it the observations instead are vectors and one defines a threshold for each component of the vector. From the components one then subtracts its threshold to form an excess vector. Note that here "excesses" can be negative. An excess vector is then considered to be a threshold exceedance if at least one of the excesses are positive, i.e., if at least one of the components exceeds its threshold. The data to be analyzed consists of the set of such threshold excess vectors. For the ILI data the observations are, e.g., the ILI rates of the three first weeks of the extreme epidemic. In the statistical analysis the data set consisting of the threshold excess vectors are assumed to be independent and identically

distributed and to follow a multivariate GP distribution. The parameters of this distribution are estimated from the data, and the estimated distribution is used for real-time prediction and for anomaly detection. Formulas and more details are given in Section 4 and in the appendix.

The philosophy behind the PoT method is that often extreme values, say high weekly ILI rates, behave quite differently than non-extreme values, and hence that only extreme values give information about other extremes. The reason for using the GP distribution is limit theory for extremes which is completely parallel to the central limit theory motivation for using the normal distribution to model "sums of errors", and that it hence provides a principled way of extrapolating outside of the range of observed data.

3 The ILI data

The nationwide Réseau Sentinelles network consists of approximately 1,500 practicing physicians in France who voluntarily participate in disease surveillance. A main part of their effort is biweekly reporting of ILI visits. The reported numbers of new cases per week are centrally converted to weekly incidence rates per 100,000 persons to obtain the "raw incidence rates" [for further details see Réseau Sentinelles, 2019]. We downloaded the raw weekly ILI incidence rates for metropolitan France from January 1985 to February 2019 and fitted the Serfling cyclic regression to estimate the seasonal weekly means. The weekly means were then subtracted from the raw weekly incidence rates to form the "deseasonalized ILI incidence rates".

Figure 1 shows the 35 epidemics which are included in the raw downloaded data. The weekly means are much smaller than the peak rates, so instead plotting the deseasonalized ILI data would not change the appearance of the graph.

In the sequel we only study the deseasonalized 1985–2018 data and put the 2019 data aside as a test case.

Epidemics are extreme events, with a behavior which is much different from the behavior during non-epidemic periods. To select the extreme part of the epidemics, we adapted the definition of the start of an annual epidemic, and also, to obtain good fit of the GP models, we applied a further selection proceedure which removed a few of the least extreme epidemics from the modelling.

Thus, we deemed an epidemic period to begin when the deseasonalized ILI rates exceeded the threshold 275 during two consecutive weeks. The start of the epidemic period was set to be the first of these two weeks, and the end was defined to be the end of the Serfling epidemic period. The resulting 35 epidemic periods had lengths varying from 3 to 12 weeks. The "size of the epidemic" was computed as the sum of the weekly deseasonalized ILI incidence rates for the weeks in the epidemic period. The threshold 275 corresponds to the 0.35 quantile of all ILI rates within a Serfling epidemic period. The choice of this threshold was driven by the wish to have a definition which made the epidemics as synchronized as possible, see Figure 2. From now on, we will refer to the first three weeks of an epidemic period as Week 1, Week 2 and Week 3.

Below we use the deseasonalized ILI rates during Weeks 1 and 2 to predict the incidence rate of Week 3. As a first step, for each of Weeks 1, 2, and 3, the 0.3 quantile of the deseasonalized ILI rates was subtracted from the rates themselves,

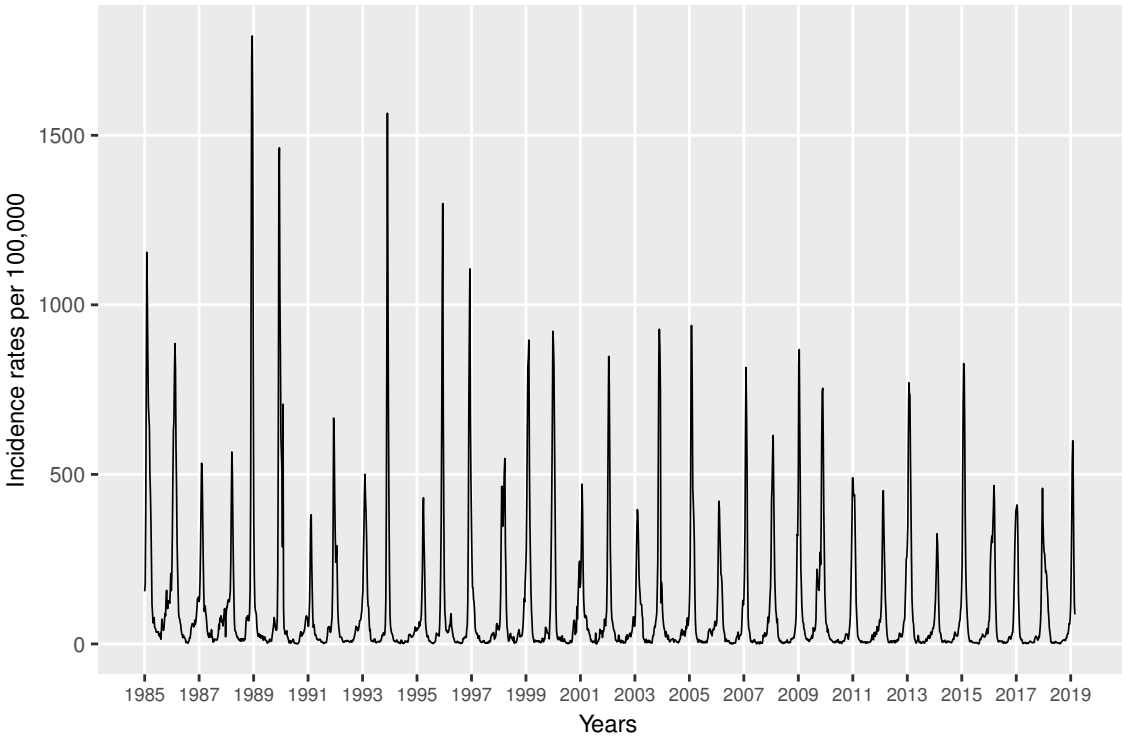

Figure 1: Weekly raw ILI incidence rates per 100,000 persons in metropolitan France from January 1985 to February 2019.

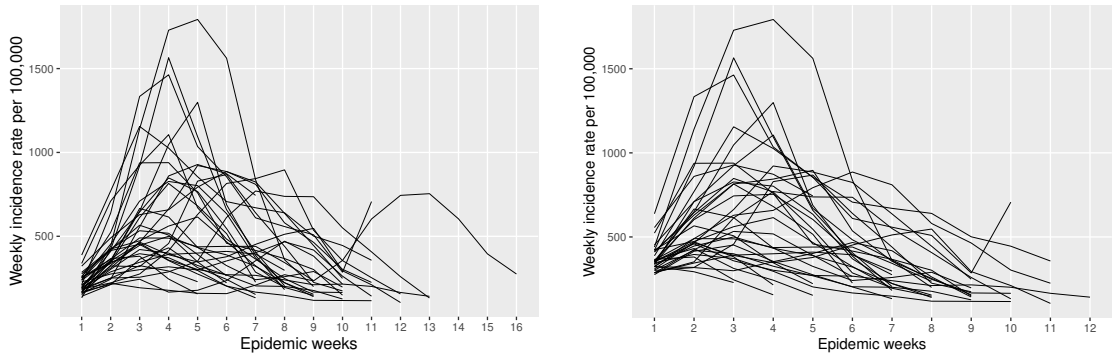

a) b)

Figure 2: a) Weekly deseasonalized ILI incidence rates for the Serfling epidemics, and b) weekly deseasonalized ILI incidence rates for epidemics obtained from the definition in this paper.

to obtain "threshold excesses" for the deseasonalized data. The values of these quantiles were Week 1: 226, Week 2: 327 and Week 3: 347. Recall that according to this definition excesses can be negative. If at least one of these three threshold excesses in an epidemic was positive, we classified this epidemic as "extreme". In this way we obtained 32 extreme epidemics. The 32 three-dimensional vectors consisting of the threshold excesses for Weeks 1, 2, and 3 in these extreme epidemics were the basis for our analysis.

We additionally used the observed incidence rates during Weeks 1 and 2 to predict the size of the epidemic. This was done in the same way as for prediction of the ILI rate of Week 3. We considered the three-dimensional vectors consisting of threshold excess ILI rates for Weeks 1 and 2, and for the size of the epidemic. Now only 31 of these vectors were considered as "extreme" (the 0.3 quantile for the size of the epidemic was equal to 1973).

The 0.3 quantile threshold was chosen, as is standard in extreme value statistics, as a compromise between model fit and the wish to have as much data as possible. As an epidemic may be considered as a deviation from the standard behaviour of ILI rates outside of an epidemic, the level 0.3 seems to be a reasonable choice.

4 Methods

Section 4.1 presents estimations of probabilities of occurence of large epidemics during future years, obtained by standard methods from EVS. This answers the question in Problem (P1). Our approach to Problem (P2), real-time forecasting, as explained in Section 4.2, consists of two steps: first a multivariate GP distribution is fitted to the threshold excesses, and then prediction is done by computing conditional probabilities of exceeding thresholds, using the fitted distribution. It builds on recent results on multivariate EVS modeling, [Rootzén et al., 2016], [Kiriliouk et al., 2019]. Section 4.3 concerns Problem (P3): we combine a general framework of anomaly detection with GP modeling.

The size of an influenza epidemic, e.g., depends on immunity and vaccination frequency in the population at risk, and it seems likely that the size of last years epidemic will influence these. Nevertheless, contrary to what is sometimes stated in the literature, there is little indication that this translates into statistical dependence between annual seasonal epidemics in France. We hence throughout assume that epidemics occurring in different years are mutually independent.

The methods we develop apply in general dimensions and for GP distributions with general margins, but we introduce them through the 3-dimensional data described above, deseasonalized ILI incidence rates of Weeks 1, 2, and 3, and deseasonalized ILI rates of Weeks 1 and 2 and the size of the epidemic, with standard exponential margins. Formulas for the general case are given in the appendix.

4.1 Prediction of risks for future years, Problem (P1)

As outlined in Section 2, the standard method to predict risks using data from earlier observed extreme events is to select a threshold u and then model the conditional distribution of the excesses (= observations$-u$) of the threshold, given that they are positive, with the GP distribution, which has cumulative distribution

function (cdf)

$$H(x) = \begin{cases} 1 - (1 + \frac{\gamma}{\sigma}x)_+^{-1/\gamma} & \text{if } \gamma \neq 0,\ x \geq 0 \\ 1 - \exp(-\frac{x}{\sigma}) & \text{if } \gamma = 0,\ x \geq 0. \end{cases} \tag{1}$$

Here $\sigma > 0$ is a scale parameter, and γ is a shape parameter which can take both positive and negative values, and the subscript $+$ indicates that the expression in parentheses should be replaced by 0 if it is negative. The parametrization is chosen so that the cdf for $\gamma = 0$ is the limit as $\gamma \to 0$ of the cdf with non-zero γ. TThe parameters of the cdf (1) of the excesses are estimated from the observed threshold excesses, in this paper using Maximum Likelihood estimation. Then, for $x > u$, F can be estimated by

$$\widehat{F}(x) = 1 - \widehat{p}_u(1 - \widehat{H}(x - u)),$$

where $\widehat{H}$ is the GP cdf (1) with parameters replaced by their estimated values and $\widehat{p}_u = 1 - \widehat{F}(u)$ is the empirical frequency of observations which exceed the threshold u [Coles, 2001].

In this paper, the observations are either the ILI rates during Week 3 or else the size of the epidemic, and there is one observation per year (counting years as the period from July 1 to June 30). We use the excesses of the 0.3 quantiles, so that $\widehat{p}_u = 0.7$ and the number of threshold excesses is $0.7 \times 34 = 24$ since the 1985–2018 ILI data covers 34 years.

Assuming independence of the annual seasonal epidemics, the empirical cdf of largest ILI rate during n years is then obtained as $\widehat{F}(x)^n = (1 - \widehat{p}_u(1 - \widehat{H}(x - u)))^n$. The risk of exceeding a large value with probability α can be measured by the $(1 - \alpha)$th quantile x_α of this empirical cdf. It is found by solving the equation $\widehat{F}(x_\alpha)^n = 1 - \alpha$. In particular, if the shape parameter of the GP distribution is 0 so that the distribution is exponential then

$$x_\alpha = u + \widehat{\sigma}\{\log \widehat{p}_u - \log(1 - (1 - \alpha)^{1/n})\}, \tag{2}$$

for α such that $\widehat{p}_u \geq 1 - (1 - \alpha)^{1/n}$.

4.2 Real time GP prediction of high level exceedances, Problem (P2)

Since data did not indicate any deviations from $\gamma = 0$, i.e. from exponential distributions, we assumed that the marginal distributions of the positive threshold excesses of the ILI rates were exponential and standardized them to be unit exponential (Section 5.1).

We now describe our approach to Problem (P2). Let $\boldsymbol{U} = (U_1, U_2, U_3)$ be a 3-dimensional random vector such that $\mathbb{E}[\mathrm{e}^{\max \boldsymbol{U}}] < \infty$, let $f_{\boldsymbol{U}}$ be the probability density function of $\boldsymbol{U}$, let f_i, F_i be the density and distribution functions, respectively, of U_i, the i-th component of $\boldsymbol{U}$, and write $\boldsymbol{x} = (x_1, x_2, x_3)$. Throughout vectors are boldface, and operations between vectors are interpreted componentwise, with 1-dimensional vectors recycled to 3-dimensional ones as needed, so that, e.g., $\max \boldsymbol{U} = \max\{U_1, U_2, U_3\}$ and $\boldsymbol{x} + \log t = (x_1 + \log t, x_2 + \log t, x_3 + \log t)$.

According to the U-representation of GP distributions ([Kiriliouk et al., 2019], Equation (3.4)), the density function $h_{\boldsymbol{U}}$ of the 3-dimensional GP distribution with standard exponential margins generated by $\boldsymbol{U}$ may be written as

$$h_{\boldsymbol{U}}(\boldsymbol{x}) = \frac{1_{\{\boldsymbol{x} \not\leq \boldsymbol{0}\}}}{\mathbb{E}[\mathrm{e}^{\max \boldsymbol{U}}]} \int_0^\infty f_{\boldsymbol{U}}(\boldsymbol{x} + \log t)\mathrm{d}t, \tag{3}$$

where the indicator function $1_{\{\boldsymbol{x}\not\leq\boldsymbol{0}\}}$ equals one if at least one of the components of $\boldsymbol{x}$ is positive, and is zero otherwise. We used generators with independent components, so that $f_{\boldsymbol{U}} = f_1 f_2 f_3$ and chose the best one from three different models which were obtained from generators with Gumbel distributions, reverse exponential distributions, and reverse Gumbel distributions for the components of $\boldsymbol{U}$. To ensure identifiability, the location parameter of the first component was set to zero. For the Gumbel distribution we used the parametrization

$$F_i(x_i) = \exp\left(-\exp\left(-\alpha_i(x_i - \beta_i)\right)\right), \qquad \alpha_j > 0,\, \beta_j \in \mathbb{R}$$

where the requirement $\mathbb{E}[\mathrm{e}^{\max \boldsymbol{U}}] < \infty$ imposes the restriction $\boldsymbol{\alpha} > \mathbf{1}$. Formulas for the densities $h_{\boldsymbol{U}}$ for the Gumbel and reverse exponential models are given in Equations (7.2) and (7.4) of [Kiriliouk et al., 2019], and for the reverse Gumbel model in the Appendix (Equation (A.1)). We used these expressions for Maximum Likelihood estimation of the parameters of the models. The numerical optimization used the R-function `optim` with the 1-dimensional integrals in the likelihoods calculated by the R-package `pracma`.

Let $\boldsymbol{X}$ be a random vector with density $h_{\boldsymbol{U}}$. By Equation (3) the conditional probability that the third component in $\boldsymbol{X}$ exceeds a level $\ell > 0$ given the values of the first two components is

$$P[X_3 \geq \ell | X_2 = x_2, X_1 = x_1] = \frac{\int_{x_3=\ell}^{\infty} 1_{\{\boldsymbol{x}\not\leq\boldsymbol{0}\}} \int_0^{\infty} f_{\boldsymbol{U}}(\boldsymbol{x} + \log t)\mathrm{d}t\mathrm{d}x_3}{\int_{x_3=-\infty}^{\infty} 1_{\{\boldsymbol{x}\not\leq\boldsymbol{0}\}} \int_0^{\infty} f_{\boldsymbol{U}}(\boldsymbol{x} + \log t)\mathrm{d}t\mathrm{d}x_3}.$$

Using Fubini's theorem and the assumption that $f_{\boldsymbol{U}} = f_1 f_2 f_3$ this simplifies to

$$P[X_3 \geq \ell | X_2 = x_2, X_1 = x_1] = \begin{cases} \frac{\int_0^{\infty} f_1(x_1+\log t) f_2(x_2+\log t)(1-F_3(\ell+\log t))\mathrm{d}t}{\int_0^{\infty} f_1(x_1+\log t) f_2(x_2+\log t)\mathrm{d}t}, & \text{if } x_1 \vee x_2 > 0 \\ \frac{\int_0^{\infty} f_1(x_1+\log t) f_2(x_2+\log t)(1-F_3(\ell+\log t))\mathrm{d}t}{\int_0^{\infty} f_1(x_1+\log t) f_2(x_2+\log t)(1-F_3(0))\mathrm{d}t}, & \text{if } x_1 \vee x_2 \leq 0, \end{cases} \tag{4}$$

with $x_1 \vee x_2 = \max\{x_1, x_2\}$.

If one or both of Weeks 1 and 2 excesses in the new epidemic are positive one knows that the epidemic will be "extreme" and uses Equation (4), with the unknown parameters in the f_i replaced by their estimated values, as forecast of the risk that the ILI rate of Week 3 in the new epidemic will exceed the level ℓ.

If instead the Week 1 and 2 excesses both are negative one does not know whether the new epidemic will be extreme or not. In this case we multiply (4) by the observed empirical probability that the epidemic will be extreme given that Weeks 1 and 2 excesses are negative, that is with

$$\frac{\#\{\text{epidemics with positive Week 3 excess and negative Weeks 1 and 2 excesses}\}}{\#\{\text{epidemics with negative Weeks 1 and 2 excesses}\}} = 0.71\,,$$

and use this as the risk forecast.

Prediction of the risk that the size of the epidemic exceeds a level was done in the same way.

Because of computational issues caused by the small number of available extreme episodes, we did not attempt to include the fact that the ILI rates in the first two extreme epidemic weeks had to exceed 275 into the models.

4.3 Detection of unusual extreme epidemics, Problem (P3)

We take advantage of the GP method for early detection of "anomalous extreme epidemics". Here anomalous is interpreted to be with respect to the fitted GP model from Section 4.2. Hence an anomaly corresponds to an unusual observation given that the ILI rates of at least one of Weeks 1, 2 or 3 is large.

Our approach is a combination of a classical framework of anomaly detection [e.g. Section 2 of Root et al., 2015] with GP modeling. A very large value of the estimated GP negative log-likelihood of the observed rates during the first three weeks of an extreme epidemic would indicate that something anomalous, and potentially very dangerous, is happening while a smaller negative log-likelihood could alleviate fears.

Recall that the GP negative log-likelihood is is given by

$$-\log h_{\boldsymbol{U}}(\boldsymbol{x}) = \log \mathbb{E}[\mathrm{e}^{\max \boldsymbol{U}}] - \log \int_0^\infty f_{\boldsymbol{U}}(\boldsymbol{x} + \log t)\mathrm{d}t,$$

for $\boldsymbol{x} \in \mathbb{R}^3$ such that $\boldsymbol{x} \not\leq \boldsymbol{0}$. We computed the value of the negative log-likelihoods of the fitted GP model for 1,500 simulated datasets and used them to obtained significance levels for the GP negative log-likelihoods (Section 6.1 below). The corresponding p-values are a measure of the extent to which an extreme epidemic is anomalous.

A pandemic occurs when a new type of virus for which there is little natural immunity is spreading. This can cause very dangerous influenza epidemics, and hence the anomality measure is particularly interesting for pandemic years, as an early indication of how France will fare during the pandemic.

5 Results: Prediction of extreme ILI loads on the health care system in France

In this section we apply the methods from Section 4 to the deseasonalized Sentinelles ILI rates.

5.1 Risk of extreme ILI incidence rates next year, and for the next 10 years

We first fitted one-dimensional GP cdf-s, Equation (1), to the positive excesses of the 0.3 quantile of the deseasonalized ILI rates of Weeks 1, 2 and 3, and to the sizes of the epidemics and made likelihood ratio tests of the hypotheses that the shape parameters γ were equal to zero. The p-values in the tests were 0.85, 0.90, 0.75, and 0.15 and gave no reason to doubt that $\gamma = 0$, i.e. that the cdf-s are exponential. The qq-plots in Figure 3 indicate good fit of the exponential distribution. We hence assumed that all γ-s equal zero during the rest of the analysis.

Standard estimates and confidence intervals for the scale parameters of the exponential distributions are given in Table 1, and quantiles calculated using Equa-

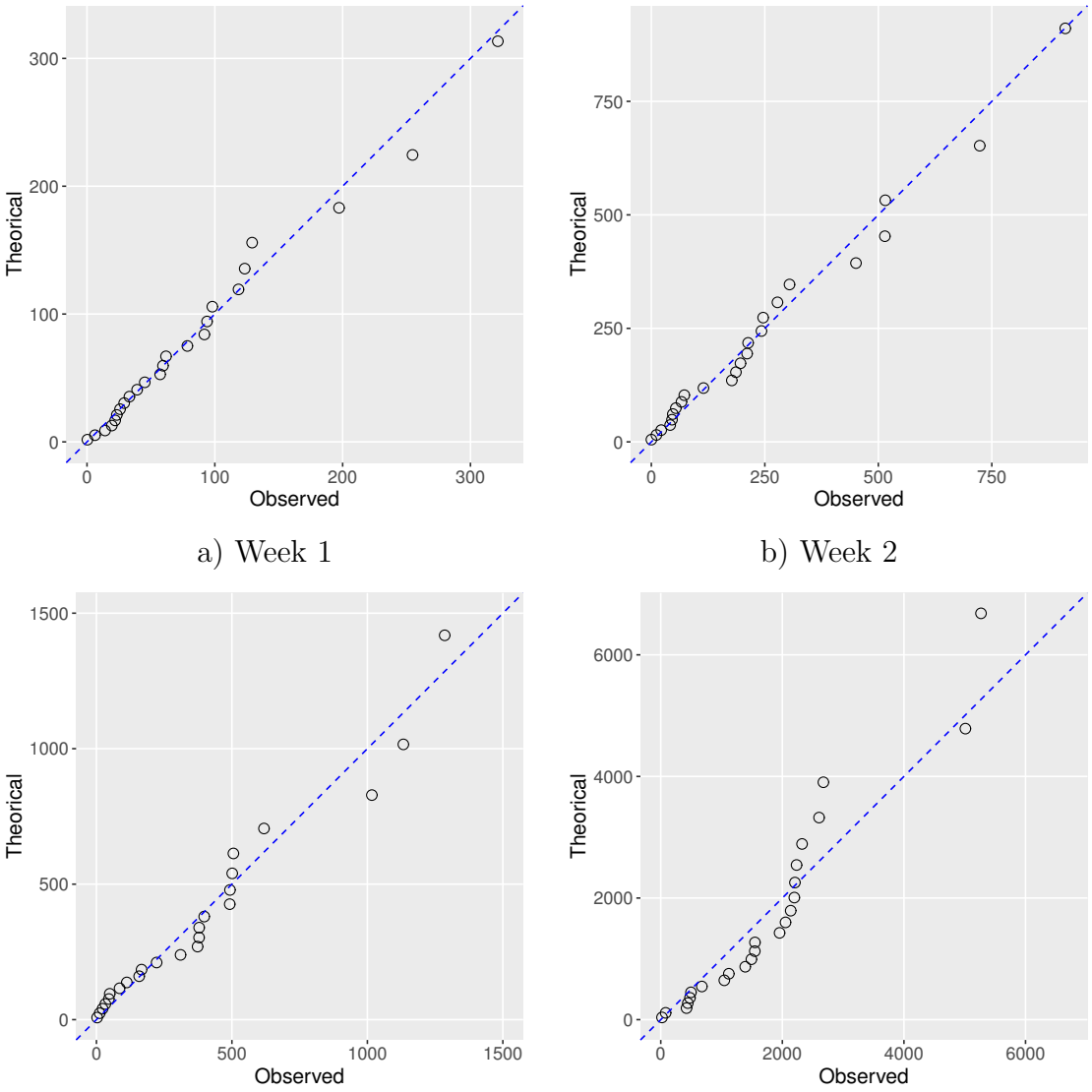

a) Week 1

b) Week 2

c) Week 3

d) Size of epidemic

Figure 3: Quantile-quantile plots of the exponential fit for the positive deseasonalized ILI incidence rate excesses of the 0.3 quantile.

Table 1: Estimates of scale parameters of the positive deseasonalized ILI rate excesses of the 0.3 quantile. CI is confidence interval.

	Week 1	Week 2	Week 3	Size of epidemic
Estimate	81	235	366	1,726
95% CI	[48 ; 114]	[141; 330]	[219 ; 513]	[1,035 ; 2,417]

Table 2: Estimated rates such that the probability that the deseasonalized ILI incidence rates exceed them is 10% or 1%.

α	one year 10%	one year 1%	10 years 10%	10 years 1%
Week 3	1,063	1,907	1,889	2,749
Size of epidemic	5,347	9,322	9,241	13,289

tion (2) in Table 2. For example, there is 10% chance that the size of the epidemic will exceed the rate 9,241 per 100,000 at least once during the next 10 years.

5.2 GP Real-time prediction of the ILI incidence rate of Week 3 and of the size of the epidemic

We first standardized the ILI excesses to unit exponential margins by dividing by the scale parameter estimates from Table 1, and then selected the best one from the three families of GP distributions listed in Section 4.2.

Table 3 shows that in terms of AIC and BIC the GP family with reverse exponential generators performed best for the ILI rates of Week 3, but that the difference to the model with Gumbel generators was not large, and that for the size of the epidemic the model with Gumbel generators was best. For computational convenience and to make results more comparable we choose to use the model with Gumbel generators both for prediction of the ILI rate of Week 3 and for prediction of the size of the epidemic. We call this model, which has Gumbel generators and standard exponential marginal distributions, the Gumbel model. It has 5 parameters, the 3 scale parameters of the 3 Gumbel generators and 2 location parameters for the generators, with the remaining location parameter fixed to ensure identifiability.

Table 4 indicated that the full model (M1) should not be simplified further. In the estimation we fixed the first location parameter β_1 to equal 0. Table 5 gives the estimated parameters for the selected Gumbel model.

Table 6, as an example, shows the predicted risk, using Equation (4) computed from the fitted GP model and using logistic regression, that the set aside 2019 epidemic should exceed the levels $(0.5, 0.75, 0.95, 1, 1.2) \times$ the largest ILI rate observed during 1985–2019. The predicted probabilities, even for the lowest level were quite small, and in fact this level was not exceeded. Logistic regression requires that

Table 3: AIC and BIC for the fit of different models a) Week 3 and b) for the size of the epidemic

Generator:	Gumbel	Reverse exponential	Reverse Gumbel
AIC	203	198	699
BIC	211	205	706

a) Week 3

Generator:	Gumbel	Reverse exponential	Reverse Gumbel
AIC	218	226	689
BIC	225	233	696

b) Size of epidemic

there is at least one level exceedance, and was not useful for predicting exceedances of the two largest levels.

Table 6: Predicted probabilities of exceedance for the 2019 epidemic. For the 2019 epidemic the ILI rate of Week 3 was 500, and the size of the epidemic was 1,192. Multiple is multiple of largest observed rate.

Multiple	0.5	0.75	0.95	1	1.2
Level	816	1,224	1,551	1,632	1,959
GP	0.038	0.002	0.0003	0.0001	0.00002
Logistic	0.018	0.018	0.011	-	-

a) Week 3

Multiple	0.5	0.75	0.95	1	1.2
Level	3,620	5,431	6,879	7,241	8,689
GP	0.096	0.017	0.004	0.003	0.0007
Logistic	0.019	0.013	0.013	-	-

b) Size of the epidemic

5.3 Quantifying the risk that an anomalous epidemic is starting

Recall that by anomalous we mean anomalous with respect to the fitted Gumbel model in Section 5.2, i.e. that the GP negative log-likelihood of a new epidemic is unusually large. The Sentinelles ILI data only includes one pandemic, the 2009 swine flu pandemic. However, surprisingly, the Gumbel model negative log-likelihood for the ILI rates of Weeks 1, 2, and 3 for the 2009-10 extreme epidemic in France was in no way unusual, see Figure 4, and hence did not point to a risk of a dangerous development. This in fact did not happen either, see Figure 1.

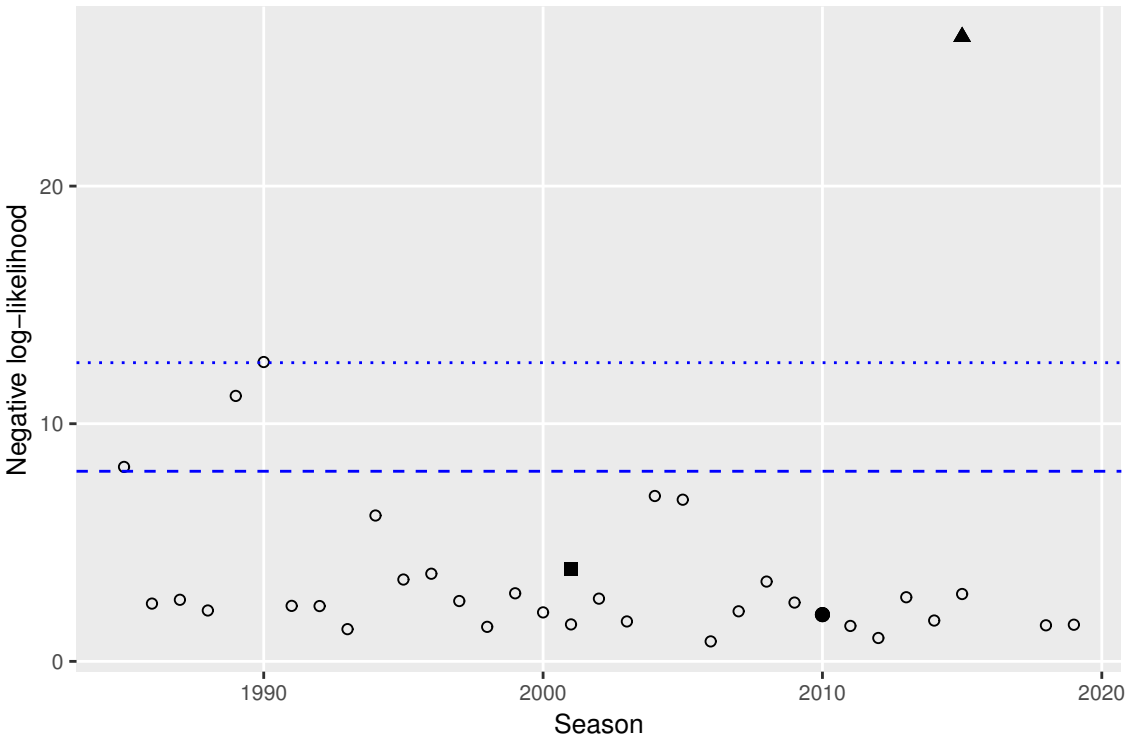

Figure 4: Leave-one-out negative Gumbel log-likelihoods for the ILI rates of Weeks 1-3 in the 33 extreme epidemics 1985 to 2019. Black circle is the 2009 pandemic, square is an added extreme point, and triangle is an added anomalous point. Dashed and dotted blue lines are the cut-offs for the 1% and 0.1% significance levels.

Table 4: AIC, BIC and LR tests for simplification of the Gumbel model a) for Week 3 and b) for the size of the epidemic.

Model	Parameters	AIC	BIC	LR p-values
M1	$\alpha_1, \alpha_2, \alpha_3, \beta_2, \beta_3$	203	211	-
M2	$\alpha_1, \alpha_2, \alpha_3$	219	226	5.13×10^{-4}
M3	α, β_2, β_3	217	224	1.15×10^{-3}
M4	α	214	215	2.84×10^{-3}

a) Week 3

Model	Parameters	AIC	BIC	LR p-values
M1	$\alpha_1, \alpha_2, \alpha_3, \beta_2, \beta_3$	218	225	-
M2	$\alpha_1, \alpha_2, \alpha_3$	227	235	8.00×10^{-3}
M3	α, β_2, β_3	226	234	1.25×10^{-2}
M4	α	222	224	2.77×10^{-2}

b) Size of epidemic

Table 5: Estimates of parameters $(\boldsymbol{\alpha}, \boldsymbol{\beta})$ for the Gumbel model a) for Week 3 and b) for the size of the epidemic.

Parameter	α_1	α_2	α_3	β_2	β_3
Estimate	2.10	6.45	3.14	0.48	0.31

a) Week 3

Parameter	α_1	α_2	α_3	β_2	β_3
Estimate	2.62	4.74	2.13	0.22	-0.11

b) Size of epidemic

There is a fine line between "extreme" and "anomalous" epidemics. To illustrate this we added two extra points to Figure 4 corresponding to an extreme epidemic obtained as i) a simulation from the Gumbel model of ILI rates of Weeks 1, 2, and 3, with the simulation chosen such that the rate of Week 3 in the simulation equals the 99% quantile of the simulated rates for Week 3, and ii) a point obtained from i) by multiplying the ILI rates of Weeks 1 and 3 by 2 and rate of Week 2 by 0.1. As expected, point ii) seems much more anomalous.

The significance levels for anomaly detection were obtained as follows: we simulated 1,500 datasets, each consisting of 33 epidemics from the selected GP model, and for each simulated dataset obtained an estimated negative log-likelihood by inserting epidemic 33 into the the negative logarithm of the Gumbel density estimated from the first 32 epidemics. The results were sorted to obtain quantiles, see Table 7. These are the cut-off levels used in Figure 4. Due to the size of the simulations there is substantial uncertainty in the estimated 99.9% quantile.

Table 7: Cut-off levels to determine significance of the negative log-likelihood of a new epidemic, with the log-likelihood computed from the Gumbel model fitted to the 32 observed extreme epidemics 1985–2018.

Significance level	10%	5%	1%	0.1%
Cut-off	5.16	6.06	8.00	12.57

6 Assessment of prediction of level exceedances

This section presents the tools we use to assess of prediction of level exceedances and their applications to the 1985–2019 ILI data.

6.1 Methods

The accuracy of probabilistic predictions depends on (i) how well one is able to model and use models for prediction, and (ii) to what extent it is possible to predict at all, i.e. on the dependence between the predictors and the event one wants to predict. There is a substantial literature on assessment of forecasting [see Lerch et al., 2017, Biggerstaff et al., 2016, and references therein]. However, with few exceptions [e.g. Renard et al., 2013], this literature provides metrics which compare predictions with observations and does not touch on the question we are interested in: prediction of exceedance of a level which is close to, or larger, than the largest observed value. The problem is that standard assessment metrics are not useful when the frequency of level exceedances in the data is small or zero.

We use Brier plots and standardized Brier scores to address (i) and (ii). The Brier plots show predicted probabilities of level exceedance stratified according to if there was an exceedance or not. The standardized Brier score is defined as

$$1 - \frac{\frac{1}{N}\sum_{i=1}^{N}(\widehat{p}_i - o_i)^2}{p(1-p)},$$

where $\widehat{p}_i$ is the predicted probability of exceedance, $o_i = 1$ if there was an exceedance, and 0 otherwise, N is the number of exceedances and $p = \frac{1}{N}\sum_{i=1}^{N} o_i$, see e.g. [Steyerberg et al., 2010]. This score is bounded by 1, with larger values indicating better prediction and equality meaning perfect prediction. Using the predictor $p_i = p$ gives the value 0.

(i) Model fit and prediction of exceedance of moderate levels: In addition to standard model checking methods we used leave-one-out cross-validation to make Brier plots and computed standardized Brier scores for the GP predictions of moderately high level exceedances for the 1985–2019 epidemics. To have a baseline to compare with we also did the same analyses for logistic regression.

(ii) Prediction outside of the range of the data: We used the simulated 1,500 data sets consisting of 33 extreme epidemics from the selected GP model for the prediction of the rate of Week 3 (recall that 32 epidemics were classified as extreme). For each simulated data set we then estimated new model parameters from the first 32 epidemics and used the resulting model to predict the ILI rate of Week 3 in the 33rd epidemic from the rates of Weeks 1 and 2 in this epidemic. We applied the same procedure for the size of the epidemic (for which 31 epidemics were extreme), but

now simulating 32 extreme epidemics. The simulations used Method 4 of [Rootzén et al., 2018, Section 7], with the tuning constant set to $K = 10^6$.

6.2 Accuracy of real-time predictions

We used the levels given in Table 6 to assess performance of the EVS real-time predictions on the 1985–2019 ILI data. Additionally, for the two lowest levels we also computed logistic regression predictions of the exceedance probabilities. Logistic regression was not useful for prediction of risks of exceedance of the three highest levels.

(i) Model fit and prediction of exceedance of moderate levels: For prediction of the ILI rate of Week 3 the 33 years with extreme epidemics (32 extreme epidemics between 1985 and 2018 plus 2019 which is also an extreme epidemic) were used for leave-one-out cross-validation of prediction accuracy and for the size of the epidemics the 32 years with extreme epidemics were used. Table 8 and Figure 5 show that both GP prediction and logistic regression performed well. The normalized Brier scores were higher for logistic regression than for the GP predictions. The differences were mainly caused by differences in the predictions for one out of the 33 (or 32) extreme epidemics.

Table 8: Standardized Brier scores obtained from leave-one-out cross-validation. Multiple is multiple of largest observed deseasonalized 1985–2019 ILI rate.

		Week 3		Size of epidemic	
	Multiple	0.5	0.75	0.5	0.75
	Level	816	1,224	3,620	5,431
Brier score	GP	0.54	0.57	0.37	0.54
	Logistic	0.77	0.72	0.75	0.68

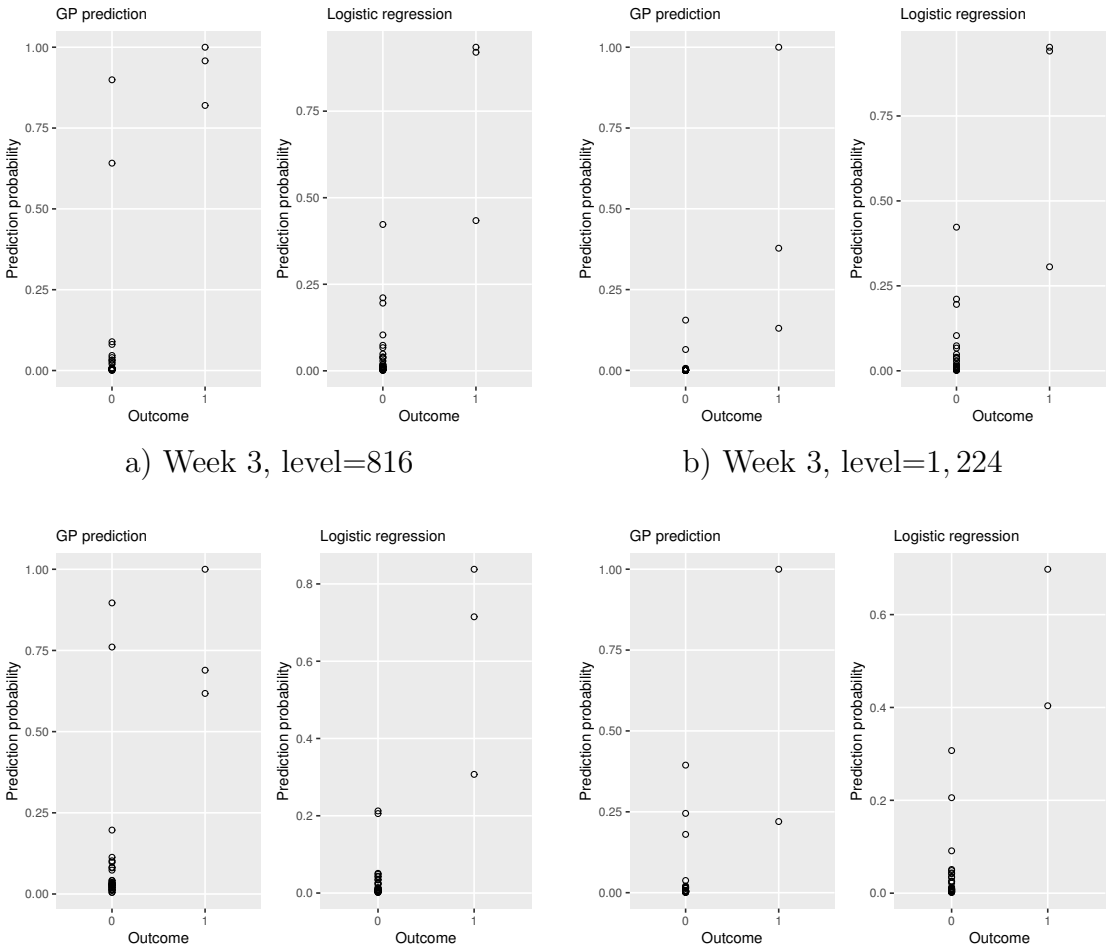

a) Week 3, level=816

b) Week 3, level=1, 224

c) Size of epidemic, level=3, 620

d) Size of epidemic, level=5, 431

Figure 5: Brier plots obtained from leave-one-out cross-validation.

(ii) Prediction outside of the range of the data: We simulated 1,500 sets of 33 extreme epidemics from the final estimated Gumbel model and for each data set fitted the Gumbel model to the first 32 epidemics and used the fitted model to predict the third week in the 33rd epidemic from the first two weeks. We applied the same procedure for the size of epidemic but now simulating 32 extreme epidemics. Figure 6 shows a similar behaviour of the simulated predictions as for the cross-validation of prediction of Week 3 which are shown in Figure 5. Similar figures (not shown) for the size of the epidemic led to the same conclusion.

The best possible prediction probability is the conditional probability in the true model. For the data, the true model of course is not known, but in simulations it is. Figure 7 and Table 9 show that the true model gives somewhat better prediction probabilities for Week 3, but that differences are quite small. Thus, perhaps surprisingly, uncertainty in parameter estimation had little influence on prediction accuracy.

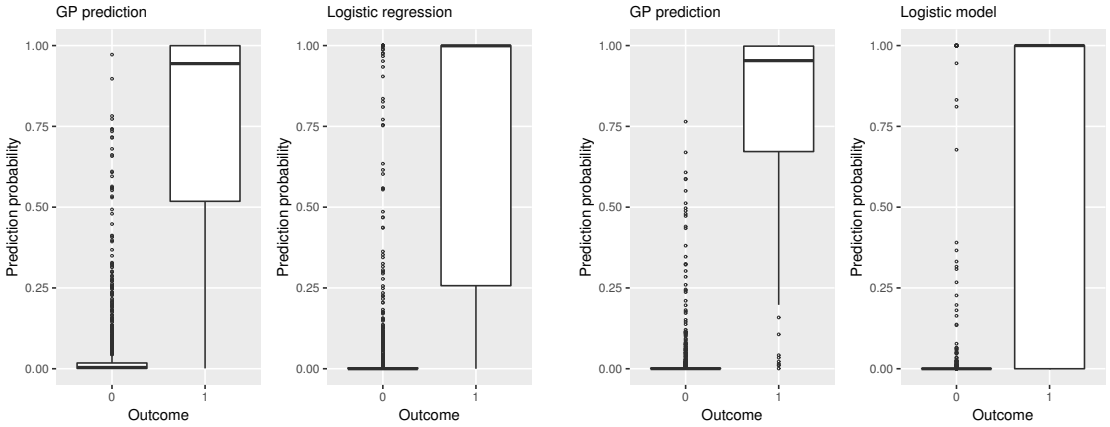

a) Week 3, level =816 b) Week 3, level=1, 224

Figure 6: Brier boxplots of the prediction probabilities obtained from simulation of the fitted Gumbel model.

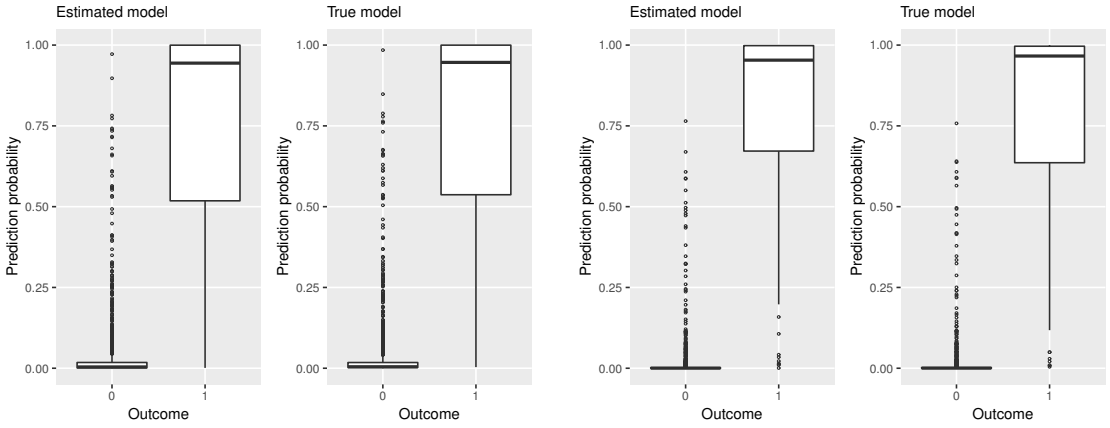

a) Week 3, level=816 b) Week 3, level=1, 224

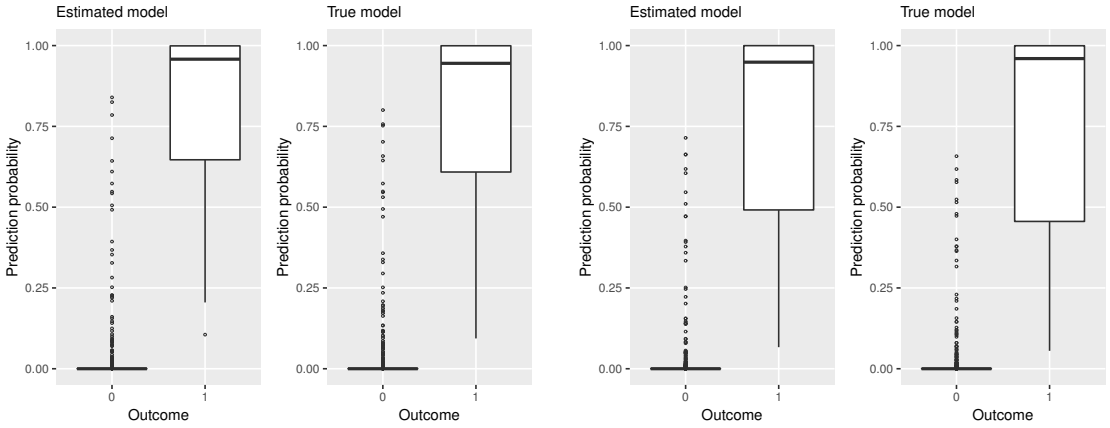

c) Week 3, level=1, 551 d) Week 3, level=1, 632

Figure 7: Brier boxplots comparing prediction probabilities obtained from using parameters estimated from the first 32 simulated extreme epidemics and obtained from using the true model parameters.

Table 9: Standardized Brier scores for the simulated data. "Multiple" is multiple of largest observed rate 1985–2019, "True" means prediction used the true model parameters.

Multiple	0.5	0.75	0.95	1	1.2
Level	816	1,224	1,551	1,632	1,959
GP	0.71	0.74	0.70	0.69	0.79
Logistic	0.47	0.27	0.01	-	-
True	0.70	0.74	0.70	0.70	0.78

a) Week 3

Multiple	0.5	0.75	0.95	1	1.2
Level	3,620	5,431	6,879	7,241	8,689
GP	0.57	0.61	0.66	0.70	0.65
Logistic	0.45	0.42	0.33	-	-
True	0.60	0.65	0.68	0.70	0.67

b) Size of the epidemic

The GP prediction method led to high Brier scores, showing that GP prediction from a Gumbel model with the parameters used in the simulations works well, see Table 9. Areas under the ROC curve (not included in paper) were all higher than 0.92, again indicating good predictions.

To judge the differences between the cross-validated Brier scores and the simulated Brier scores we used the simulations to construct 4 data sets parallel to the observed extreme epidemics and computed cross-validated normalized Brier scores for each of these. The random variations between the resulting 4 sets of Brier scores were larger than the differences between Table 8 and Table 9.

7 Discussion and conclusions

Extreme value statistics is a body of theoretically motivated and consistent methods for estimation and prediction of risks of threshold exceedances. Using EVS is important for providing methods which generalize and allow for comparison between results obtained in separate studies.

Section 4.1 provides estimates of risks that large — or very large — influenza epidemics will occur in years to come. These estimates provide input for long term resource planning and are standard in other areas such as environmental science, but have so far been little used in epidemiology and health care planning.

For levels inside the range of observed values many real-time prediction methods, such as logistic regression, are available and often work well, and logistic regression also does this for prediction of risks of level exceedances of ILI incidence rates. However, these methods cannot handle levels which are close to or above the largest observed values, which often are the most important ones. The results of Section 5.2 indicate that, provided the GP distribution continues to hold outside of the range of data, the GP real-time prediction method can provide useful predictions of risks

of exceedance of such very high levels.

Advances in medical technology will aid handling of risks of occurrence of new and extremely dangerous pandemics, but instead the fast rise in air travel makes risks of very rapid spread much more dramatic than it was during the time of the Spanish Flu. The methods developed in Section 6.2 provide a new way to judge risks associated with a developing pandemic.

Future development of the methods introduced in this paper will profit from the very rapid advance of the theory of multivariate extremes, including improved numerical methods and the development of statistical techniques.

Finally, both real-time prediction of risks of exceeding very high thresholds and detection of anomalies are important much more broadly in health care and also in very many other areas. The methods we have developed will be useful also in these areas.

Acknowledgment

We thank Tom Britton, Anna Kiriliouk, Thordis Torainsdottir and Jenny Wadsworth for help and comments. Research supported by the Knut and Alice Wallenberg foundation.

Appendix

Probability density function for the 3-dimensional GP distribution with reverse Gumbel distributions

The generator of the third model used in Sections 4.2 and 5.2 has independent reverse Gumbel distributed components with distribution functions

$$F_j(x_j) = 1 - \exp[-\exp\{\alpha_j(x_j - \beta_j)\}], \qquad \alpha_j > 0,\, \beta_j \in \mathbb{R}.$$

Calculations very similar to the derivation of Equation (7.2) in [Kiriliouk et al., 2019] show that the resulting GP distribution has probability density function

$$h_{\boldsymbol{U}}(\boldsymbol{x}, \mathbf{1}, \mathbf{0}) = \frac{\int_0^\infty \prod_{i=1}^d \alpha_j \left(t\mathrm{e}^{x_j-\beta_j}\right)^{\alpha_j} \exp\left(-\left(t\mathrm{e}^{x_j-\beta_j}\right)^{\alpha_j}\right) \mathrm{d}t}{\int_0^\infty \left(1 - \prod_{i=1}^n \mathrm{e}^{-(t\mathrm{e}^{-\beta_j})^{\alpha_j}}\right) \mathrm{d}t}. \tag{A.1}$$

Conditional prediction of extreme events

Generalizing the notation in Section 4.2, write $\boldsymbol{x}_{i:j} = (x_i, \ldots, x_j)$ and $\boldsymbol{x} = (x_1, \ldots, x_d)$. Then, using the same conventions as in Section 4.2, the U-representation of the density of d-dimensional GP distributions is

$$h_{\boldsymbol{U}}(\boldsymbol{x}) = h_{\boldsymbol{U}}(\boldsymbol{x}; \boldsymbol{\sigma}, \boldsymbol{\gamma}) = \frac{1_{\{\boldsymbol{x} \not\leq \mathbf{0}\}}}{\mathbb{E}[\mathrm{e}^{\max \boldsymbol{U}}]} \left(\prod_{j=1}^d \frac{1}{\sigma_j + \gamma_j x_j}\right) \int_0^\infty f_{\boldsymbol{U}}\left(\frac{1}{\boldsymbol{\gamma}} \log\left(1 + \boldsymbol{\gamma}\frac{\boldsymbol{x}}{\boldsymbol{\sigma}}\right) + \log t\right) \mathrm{d}t$$

Note that in the general case $h_{\boldsymbol{U}}$ depends both on the generator $\boldsymbol{U}$ and on the marginal parameters $\boldsymbol{\sigma}, \boldsymbol{\gamma}$. For $\boldsymbol{\sigma} = \mathbf{1}, \boldsymbol{\gamma} = \mathbf{0}$ this expression reduces to Equation (3). The next proposition gives the conditional prediction formulas for prediction of the exceedances of the dth component given the first c components of a d-dimensional vector.

Proposition 1. *Let* $\mathbf{X} = (X_1, \ldots, X_d)$ *a* d*-dimensional GP vector with density* $f_{\boldsymbol{U}}$ *and let* $1 \leq c < d$*. The probability that* X_d *will exceed a threshold* v *given* $\boldsymbol{X}_{1:c} = \boldsymbol{x}_{1:c}$ *is given by*

i) for $\boldsymbol{x}_{1:c} \not\leq 0$ *and* $v \in \mathbb{R}$

$$\mathbb{P}[X_d > v \mid \boldsymbol{X}_{1:c} = \boldsymbol{x}_{1:c}] = \begin{cases} \dfrac{\int_{x_d > v} \int_{\boldsymbol{x}_{c+1:d-1}} \phi(\boldsymbol{x}) \mathrm{d}\boldsymbol{x}_{c+1:d-1} \mathrm{d}x_d}{\int_{\boldsymbol{x}_{c+1:d-1}} \phi(\boldsymbol{x}) \mathrm{d}\boldsymbol{x}_{c+1:d}} & \text{if } c < d-1 \\ \dfrac{\int_{x_d > v} \phi(\boldsymbol{x}) \mathrm{d}x_d}{\int_{\boldsymbol{x}_d} \phi(\boldsymbol{x}) \mathrm{d}\boldsymbol{x}_{c+1:d}} & \text{if } c = d-1; \end{cases}$$

ii) for $\boldsymbol{x}_{1:c} \leq 0$ *and* $v > 0$

$$\mathbb{P}[X_d > v \mid \boldsymbol{X}_{1:c} = \boldsymbol{x}_{1:c}] = \begin{cases} \dfrac{\int_{x_d > v} \int_{\boldsymbol{x}_{c+1:d-1}} \phi(\boldsymbol{x}) \mathrm{d}\boldsymbol{x}_{c+1:d-1} \mathrm{d}x_d}{\int_{\boldsymbol{x}_{c+1:d-1} \not\leq \mathbf{0}} \phi(\boldsymbol{x}) \mathrm{d}\boldsymbol{x}_{c+1:d-1}} & \text{if } c < d-1 \\ \dfrac{\int_{x_d > v} \phi(\boldsymbol{x}) \mathrm{d}x_d}{\int_{x_d > 0} \phi(\boldsymbol{x}) \mathrm{d}x_d} & \text{if } c = d-1; \end{cases}$$

iii) for $\boldsymbol{x}_{1:c} \leq 0$ *and* $v \leq 0$

$$\mathbb{P}[X_d > v \mid \boldsymbol{X}_{1:c} = \boldsymbol{x}_{1:c}] = \begin{cases} \dfrac{\int_{x_d > 0} \int_{\boldsymbol{x}_{c+1:d-1} \leq \mathbf{0}} \phi(\boldsymbol{x}) \mathrm{d}\boldsymbol{x}_{c+1:d-1} \mathrm{d}x_d}{\int_{\boldsymbol{x}_{c+1:d-1} \not\leq \mathbf{0}} \phi(\boldsymbol{x}) \mathrm{d}\boldsymbol{x}_{c+1:d-1}} \\ + \dfrac{\int_{x_d > v} \int_{\boldsymbol{x}_{c+1:d-1} \not\leq \mathbf{0}} \phi(\boldsymbol{x}) \mathrm{d}\boldsymbol{x}_{c+1:d-1} \mathrm{d}x_d}{\int_{\boldsymbol{x}_{c+1:d-1} \not\leq \mathbf{0}} \phi(\boldsymbol{x}) \mathrm{d}\boldsymbol{x}_{c+1:d-1}} & \text{if } c < d-1 \\ 1 & \text{if } c = d-1. \end{cases}$$

Example. For $d = 3$ and $c = 2$ we get

$$\mathbb{P}\left[X_3 > v_3 \mid \mathbf{X}_{1:2} = \mathbf{x}_{1:2}\right] = \begin{cases} \dfrac{\int_{x_3 > v_3} \phi(\boldsymbol{x}) \mathrm{d}x_3}{\int_{x_3} \phi(\boldsymbol{x}) \mathrm{d}x_3} & \text{if } \mathbf{x}_{1:2} \not\leq \mathbf{0} \text{ and } v_3 \in \mathbb{R}; \\ \dfrac{\int_{x_3 > v_3} \phi(\boldsymbol{x}) \mathrm{d}x_3}{\int_{x_3 > 0} \phi(\boldsymbol{x}) \mathrm{d}x_3} & \text{if } \mathbf{x}_{1:2} \leq \mathbf{0} \text{ and } v_3 > 0; \\ 1 & \text{if } \mathbf{x}_{1:2} \leq \mathbf{0} \text{ and } v_3 \leq 0. \end{cases}$$

Proof. Let $f_{x_d | \boldsymbol{X}_{1:c} = \boldsymbol{x}_{1:c}}$ be the conditional marginal density of x_d given $\boldsymbol{X}_{1:c} = \boldsymbol{x}_{1:c}$, that is

$$f_{x_d | \boldsymbol{X}_{1:c} = \boldsymbol{x}_{1:c}}(x_d) = \frac{h_{(\boldsymbol{x}_{1:c}, x_d)}(\boldsymbol{x}_{1:c}, x_d)}{h_{\boldsymbol{x}_{1:c}}(\boldsymbol{x}_{1:c})}$$

where $h_{(\boldsymbol{x}_{1:c}, x_d)}$ is the marginal joint density of $(\boldsymbol{x}_{1:c}, x_d)$ and $h_{\boldsymbol{x}_{1:c}}$ is the marginal joint density of $\boldsymbol{x}_{1:c}$. Then,

$$\mathbb{P}[X_d > v \mid \boldsymbol{X}_{1:c} = \boldsymbol{x}_{1:c}] = \int_{x_d = v}^{\infty} f_{x_d | \boldsymbol{X}_{1:c} = \boldsymbol{x}_{1:c}}(x_d) \mathrm{d}x_d \ .$$

We start by deriving the formula for $h_{\boldsymbol{x}_{1:c}}$ and $h_{(\boldsymbol{x}_{1:c},x_d)}$. First,

$$\begin{aligned}
&h_{\boldsymbol{x}_{1:c}}(\boldsymbol{x}_{1:c}) \\
&= \int_{\boldsymbol{x}_{c+1:d}} 1_{\{\boldsymbol{x}\not\leq\boldsymbol{0}\}}\phi(\boldsymbol{x})\mathrm{d}\boldsymbol{x}_{c+1:d} \\
&= 1_{\{\boldsymbol{x}_{1:c}\not\leq\boldsymbol{0}\}}\int_{\boldsymbol{x}_{c+1:d}} \phi(\boldsymbol{x})\mathrm{d}\boldsymbol{x}_{c+1:d} + \int_{\boldsymbol{x}_{c+1:d}} 1_{\{\boldsymbol{x}_{c+1:d}\not\leq\boldsymbol{0}\}}\phi(\boldsymbol{x})\mathrm{d}\boldsymbol{x}_{c+1:d} \\
&\quad -1_{\{\boldsymbol{x}_{1:c}\not\leq\boldsymbol{0}\}}\int_{\boldsymbol{x}_{c+1:d}} 1_{\{\boldsymbol{x}_{c+1:d}\not\leq\boldsymbol{0}\}}\phi(\boldsymbol{x})\mathrm{d}\boldsymbol{x}_{c+1:d} \\
&= 1_{\{\boldsymbol{x}_{1:c}\not\leq\boldsymbol{0}\}}\int_{\boldsymbol{x}_{c+1:d}} 1_{\{\boldsymbol{x}_{c+1:d}\leq\boldsymbol{0}\}}\phi(\boldsymbol{x})\mathrm{d}\boldsymbol{x}_{c+1:d} + \int_{\boldsymbol{x}_{c+1:d}} 1_{\{\boldsymbol{x}_{c+1:d}\not\leq\boldsymbol{0}\}}\phi(\boldsymbol{x})\mathrm{d}\boldsymbol{x}_{c+1:d} \ .
\end{aligned}$$

Similarly, we show that, if $c < d-1$,

$$\begin{aligned}
h_{(\boldsymbol{x}_{1:c},x_d)}(\boldsymbol{x}_{1:c},x_d) &= 1_{\{(\boldsymbol{x}_{1:c},x_d)\not\leq\boldsymbol{0}\}}\int_{\boldsymbol{x}_{c+1:d-1}} 1_{\{\boldsymbol{x}_{c+1:d-1}\leq\boldsymbol{0}\}}\phi(\boldsymbol{x})\mathrm{d}\boldsymbol{x}_{c+1:d-1} \\
&\quad + \int_{\boldsymbol{x}_{c+1:d-1}} 1_{\{\boldsymbol{x}_{c+1:d-1}\not\leq\boldsymbol{0}\}}\phi(\boldsymbol{x})\mathrm{d}\boldsymbol{x}_{c+1:d-1} \ .
\end{aligned}$$

If $c = d-1$, then

$$h_{(\boldsymbol{x}_{1:c},x_d)}(\boldsymbol{x}_{1:c},x_d) = h_{\boldsymbol{U}}(\boldsymbol{x}) = 1_{\{\boldsymbol{x}\not\leq\boldsymbol{0}\}}\phi(\boldsymbol{x}) \ .$$

We now discuss according to the sign of $\boldsymbol{x}_{1:c}$ and v.

Case 1: $\boldsymbol{x}_{1:c} \not\leq \boldsymbol{0}$

$$h_{\boldsymbol{x}_{1:c}}(\boldsymbol{x}_{1:c}) = \int_{\boldsymbol{x}_{c+1:d}} \phi(\boldsymbol{x})\mathrm{d}\boldsymbol{x}_{c+1:d}\,,$$

and, if $c < d-1$,

$$\begin{aligned}
h_{(\boldsymbol{x}_{1:c},x_d)}(\boldsymbol{x}_{1:c},x_d) &= \int_{\boldsymbol{x}_{c+1:d-1}} 1_{\{\boldsymbol{x}_{c+1:d-1}\leq\boldsymbol{0}\}}\phi(\boldsymbol{x})\mathrm{d}\boldsymbol{x}_{c+1:d-1} \\
&\quad + \int_{\boldsymbol{x}_{c+1:d-1}} 1_{\{\boldsymbol{x}_{c+1:d-1}\not\leq\boldsymbol{0}\}}\phi(\boldsymbol{x})\mathrm{d}\boldsymbol{x}_{c+1:d-1} \ .
\end{aligned}$$

Whence,

$$h_{(\boldsymbol{x}_{1:c},x_d)}(\boldsymbol{x}_{1:c},x_d) = \begin{cases} \int_{\boldsymbol{x}_{c+1:d-1}} \phi(\boldsymbol{x})\mathrm{d}\boldsymbol{x}_{c+1:d-1} & \text{if } c < d-1 \\ \phi(\boldsymbol{x}) & \text{if } c = d-1 \ . \end{cases}$$

Therefore,

$$f_{x_d|\boldsymbol{X}_{1:c}=\boldsymbol{x}_{1:c}}(x_d) = \begin{cases} \dfrac{\int_{\boldsymbol{x}_{c+1:d-1}} \phi(\boldsymbol{x})\mathrm{d}\boldsymbol{x}_{c+1:d-1}}{\int_{\boldsymbol{x}_{c+1:d}} \phi(\boldsymbol{x})\mathrm{d}\boldsymbol{x}_{c+1:d}} & \text{if } c < d-1 \\ \dfrac{\phi(\boldsymbol{x})}{\int_{\boldsymbol{x}_d} \phi(\boldsymbol{x})\mathrm{d}\boldsymbol{x}_d} & \text{if } c = d-1. \end{cases}$$

and

$$\begin{aligned}\mathbb{P}[X_d > v \mid \boldsymbol{x}_{1:c} = \boldsymbol{x}_{1:c}] &= \int_{x_d} 1_{\{X_d>v\}} f_{x_d|\boldsymbol{X}_{1:c}=\boldsymbol{x}_{1:c}}(x_d)\mathrm{d}x_d \\ &= \begin{cases} \frac{\int_{x_d} 1_{\{X_d>v\}} \int_{\boldsymbol{x}_{c+1:d-1}} \phi(\boldsymbol{x})\mathrm{d}\boldsymbol{x}_{c+1:d-1}\mathrm{d}x_d}{\int_{\boldsymbol{x}_{c+1:d}} \phi(\boldsymbol{x})\mathrm{d}\boldsymbol{x}_{c+1:d}} & \text{if } c < d-1 \\ \frac{\int_{x_d} 1_{\{X_d>v\}}\phi(\boldsymbol{x})\mathrm{d}x_d}{\int_{\boldsymbol{x}_d}\phi(\boldsymbol{x})\mathrm{d}\boldsymbol{x}_d} & \text{if } c = d-1. \end{cases}\end{aligned}$$

Case 2: $\boldsymbol{x}_{1:c} \leq \mathbf{0}$

$$h_{\boldsymbol{x}_{1:c}}(\boldsymbol{x}_{1:c}) = \int_{\boldsymbol{x}_{c+1:d}} 1_{\{\boldsymbol{x}_{c+1:d}\not\leq\mathbf{0}\}}\phi(\boldsymbol{x})\mathrm{d}\boldsymbol{x}_{c+1:d}\,,$$

and

$$\begin{aligned}&h_{(\boldsymbol{x}_{1:c},x_d)}(\boldsymbol{x}_{1:c}, x_d) \\ &= \begin{cases} 1_{\{x_d>0\}} \int_{\boldsymbol{x}_{c+1:d-1}} 1_{\{\boldsymbol{x}_{c+1:d-1}\leq\mathbf{0}\}}\phi(\boldsymbol{x})\mathrm{d}\boldsymbol{x}_{c+1:d-1} & \\ \quad + \int_{\boldsymbol{x}_{c+1:d-1}} 1_{\{\boldsymbol{x}_{c+1:d-1}\not\leq\mathbf{0}\}}\phi(\boldsymbol{x})\mathrm{d}\boldsymbol{x}_{c+1:d-1} & \text{if } c < d-1 \\ 1_{\{x_d>0\}}\phi(\boldsymbol{x}) & \text{if } c = d-1. \end{cases}\end{aligned}$$

Therefore,

$$f_{x_d|\boldsymbol{X}_{1:c}=\boldsymbol{x}_{1:c}}(x_d) = \begin{cases} \frac{1_{\{x_d>0\}} \int_{\boldsymbol{x}_{c+1:d-1}} 1_{\{\boldsymbol{x}_{c+1:d-1}\leq\mathbf{0}\}}\phi(\boldsymbol{x})\mathrm{d}\boldsymbol{x}_{c+1:d-1}}{\int_{\boldsymbol{x}_{c+1:d}} 1_{\{\boldsymbol{x}_{c+1:d}\not\leq\mathbf{0}\}}\phi(\boldsymbol{x})\mathrm{d}\boldsymbol{x}_{c+1:d}} & \\ \quad + \frac{\int_{\boldsymbol{x}_{c+1:d-1}} 1_{\{\boldsymbol{x}_{c+1:d-1}\not\leq\mathbf{0}\}}\phi(\boldsymbol{x})\mathrm{d}\boldsymbol{x}_{c+1:d-1}}{\int_{\boldsymbol{x}_{c+1:d}} 1_{\{\boldsymbol{x}_{c+1:d}\not\leq\mathbf{0}\}}\phi(\boldsymbol{x})\mathrm{d}\boldsymbol{x}_{c+1:d}} & \text{if } c < d-1 \\ \frac{1_{\{x_d>0\}}\phi(\boldsymbol{x})}{\int_{x_d} 1_{\{x_d>0\}}\phi(\boldsymbol{x})\mathrm{d}x_d} & \text{if } c = d-1. \end{cases}$$

and

$$\begin{aligned}&\mathbb{P}[X_d > v \mid \boldsymbol{X}_{1:c} = \boldsymbol{x}_{1:c}] \\ &= \int_{x_d} 1_{\{X_d>v\}} f_{X_d|\boldsymbol{X}_{1:c}=\boldsymbol{x}_{1:c}}(x_d)\mathrm{d}x_d \\ &= \begin{cases} \frac{\int_{x_d} 1_{\{X_d>v\}}1_{\{x_d>0\}} \int_{\boldsymbol{x}_{c+1:d-1}} 1_{\{\boldsymbol{x}_{c+1:d-1}\leq\mathbf{0}\}}\phi(\boldsymbol{x})\mathrm{d}\boldsymbol{x}_{c+1:d-1}\mathrm{d}x_d}{\int_{\boldsymbol{x}_{c+1:d}} 1_{\{\boldsymbol{x}_{c+1:d}\not\leq\mathbf{0}\}}\phi(\boldsymbol{x})\mathrm{d}\boldsymbol{x}_{c+1:d}} & \\ \quad + \frac{\int_{x_d} 1_{\{X_d>v\}} \int_{\boldsymbol{x}_{c+1:d-1}} 1_{\{\boldsymbol{x}_{c+1:d-1}\not\leq\mathbf{0}\}}\phi(\boldsymbol{x})\mathrm{d}\boldsymbol{x}_{c+1:d-1}\mathrm{d}x_d}{\int_{\boldsymbol{x}_{c+1:d}} 1_{\{\boldsymbol{x}_{c+1:d}\not\leq\mathbf{0}\}}\phi(\boldsymbol{x})\mathrm{d}\boldsymbol{x}_{c+1:d}} & \text{if } c < d-1 \\ \frac{\int_{x_d} 1_{\{x_d>v\}}1_{\{x_d>0\}}\phi(\boldsymbol{x})\mathrm{d}x_d}{\int_{x_d} 1_{\{x_d>0\}}\phi(\boldsymbol{x})\mathrm{d}x_d} & \text{if } c = d-1. \end{cases}\end{aligned}$$

Now, separating according to the sign of the threshold v, we get the following cases.

Case 2.1: $v > 0$ **(with** $\boldsymbol{x}_{1:c} \leq \mathbf{0}$**)**

$$
\begin{aligned}
&\mathbb{P}[X_d > v \mid \boldsymbol{X}_{1:c} = \boldsymbol{x}_{1:c}] \\
&= \begin{cases}
\dfrac{\int_{x_d} 1_{\{X_d > v\}} \int_{\boldsymbol{x}_{c+1:d-1}} 1_{\{\boldsymbol{x}_{c+1:d-1} \leq \mathbf{0}\}} \phi(\boldsymbol{x}) \mathrm{d}\boldsymbol{x}_{c+1:d-1} \mathrm{d}x_d}{\int_{\boldsymbol{x}_{c+1:d}} 1_{\{\boldsymbol{x}_{c+1:d} \not\leq \mathbf{0}\}} \phi(\boldsymbol{x}) \mathrm{d}\boldsymbol{x}_{c+1:d}} & \\
\quad + \dfrac{\int_{x_d} 1_{\{X_d > v\}} \int_{\boldsymbol{x}_{c+1:d-1}} 1_{\{\boldsymbol{x}_{c+1:d-1} \not\leq \mathbf{0}\}} \phi(\boldsymbol{x}) \mathrm{d}\boldsymbol{x}_{c+1:d-1} \mathrm{d}x_d}{\int_{\boldsymbol{x}_{c+1:d}} 1_{\{\boldsymbol{x}_{c+1:d} \not\leq \mathbf{0}\}} \phi(\boldsymbol{x}) \mathrm{d}\boldsymbol{x}_{c+1:d}} & \text{if } c < d-1 \\
\dfrac{\int_{x_d} 1_{\{x_d > v\}} \phi(\boldsymbol{x}) \mathrm{d}x_d}{\int_{x_d} 1_{\{x_d > 0\}} \phi(\boldsymbol{x}) \mathrm{d}x_d} & \text{if } c = d-1.
\end{cases} \\
&= \begin{cases}
\dfrac{\int_{x_d} 1_{\{X_d > v\}} \int_{\boldsymbol{x}_{c+1:d-1}} \phi(\boldsymbol{x}) \mathrm{d}\boldsymbol{x}_{c+1:d-1} \mathrm{d}x_d}{\int_{\boldsymbol{x}_{c+1:d}} 1_{\{\boldsymbol{x}_{c+1:d} \not\leq \mathbf{0}\}} \phi(\boldsymbol{x}) \mathrm{d}\boldsymbol{x}_{c+1:d}} & \text{if } c < d-1 \\
\dfrac{\int_{x_d} 1_{\{x_d > v\}} \phi(\boldsymbol{x}) \mathrm{d}x_d}{\int_{x_d} 1_{\{x_d > 0\}} \phi(\boldsymbol{x}) \mathrm{d}x_d} & \text{if } c = d-1.
\end{cases}
\end{aligned}
$$

Case 2.2: $v < 0$ **(with** $\boldsymbol{x}_{1:c} \leq \mathbf{0}$**)**

$$
\begin{aligned}
&\mathbb{P}[X_d > v \mid \boldsymbol{x}_{1:c} = \boldsymbol{x}_{1:c}] \\
&= \int_{x_d} 1_{\{X_d > v\}} f_{x_d \mid \boldsymbol{X}_{1:c} = \boldsymbol{x}_{1:c}}(x_d) \mathrm{d}x_d \\
&= \begin{cases}
\dfrac{\int_{x_d} 1_{\{x_d > 0\}} \int_{\boldsymbol{x}_{c+1:d-1}} 1\{\boldsymbol{x}_{c+1:d-1} \leq \mathbf{0}\} \phi(\boldsymbol{x}) \mathrm{d}\boldsymbol{x}_{c+1:d-1} \mathrm{d}x_d}{\int_{\boldsymbol{x}_{c+1:d}} 1_{\{\boldsymbol{x}_{c+1:d} \not\leq \mathbf{0}\}} \phi(\boldsymbol{x}) \mathrm{d}\boldsymbol{x}_{c+1:d}} & \\
\quad + \dfrac{\int_{x_d} 1_{\{X_d > v\}} \int_{\boldsymbol{x}_{c+1:d-1}} 1_{\{\boldsymbol{x}_{c+1:d-1} \not\leq \mathbf{0}\}} \phi(\boldsymbol{x}) \mathrm{d}\boldsymbol{x}_{c+1:d-1} \mathrm{d}x_d}{\int_{\boldsymbol{x}_{c+1:d}} 1_{\{\boldsymbol{x}_{c+1:d} \not\leq \mathbf{0}\}} \phi(\boldsymbol{x}) \mathrm{d}\boldsymbol{x}_{c+1:d}} & \text{if } c < d-1 \\
1 & \text{if } c = d-1.
\end{cases}
\end{aligned}
$$

□

References

M. Biggerstaff, D. Alper, M. Dredze, S. Fox, I. C.-H. Fung, K. S. Hickmann, B. Lewis, R. Rosenfeld, J. Shaman, M.-H. Tsou, P. Velardi1, A. Vespignanil, and L. Finelli1. Results from the centers for disease control and prevention's predict the 2013–2014 influenza season challenge. *BMC Infectious Diseases*, 16: 357–367, 2016.

J. Bresee and F. Hayden. Epidemic influenza-responding to the expected but unpredictable. *The New England Journal of Medecine*, 368(7):589–92, 2013.

J. Chen, X. Lei, L. Zhang, and B. Peng. Using extreme value theory approaches to forecast the probability of outbreak of highly pathogenic influenza in Zhejiang, China. *PLoS ONE*, 10(2), 2015.

S. Coles. *An introduction to statistical modeling of extremes values*. Springer-Verlag, London, 2001.

R. A. Davis, P. Zang, and T. Zheng. Sparse vector autoregressive modeling. *Journal of Computational and Graphical Statistics*, 25(4):1077–1096, 2016.

P. Embrechts, C. Klüpperberg, and T. Mikosch. *Modelling extremal events for insurance and finance*. Springer Verlag, Berlin, 1997.

A. Guillou and Y. Kratz, M. Le Strat. An extreme value theory approach for the early detection of time clusters with application to the surveillance of Salmonella. *Statistics Applications*, 2013.

R. Katz, M. Parlange, and P. Naveau. Statistics of extremes in hydrology. *Advances in Water Resources*, 25:1287–1304, 2002.

A. Kiriliouk, H. Rootzén, J. Segers, and J. L. Wadsworth. Peaks over thresholds modeling with multivariate generalized Pareto distributions. *Technometrics*, 61: 123–135, 2019.

Y. Le Strat and F. Carrat. Monitoring epidemiologic surveillance data using hidden markov models. *Statistics in medicine*, 18(24):3463–3478, 1999.

S. Lerch, T. Thorarinsdottir, F. Ravazzolo, and T. Gneiting. Forecaster's dilemma: Extreme events and forecast evaluation. *Statist. Sci.*, 32(3):106–127, 2017.

A. Rambaut, N. M. Pybus, O.G., C. Viboud, J. Taubenberger, and E. Holmes. The genomic and epidemiological dynamics of human influenza a virus. *Nature*, 453 (7195):615–619, 2008.

B. Renard, K. Kochanek, M. Lang, F. Garavaglia, E. Paquet, L. Neppel, K. Najib, J. Carreau, P. Arnaud, Y. Aubert, F. Borchi, J.-M. Soubeyroux, S. S. Jourdain, J.-M. X Veysseire, E. Sauquet, T. Cipriani, and A. Auffray. Data-based comparison of frequency analysis methods: A general framework. *Water Resources Research*, 49:825–843, 2013.

Réseau Sentinelles. Inserm/Sorbonne Université. `https://www.sentiweb.fr`, 2019.

J. Root, J. Qian, and V. Saligrama. Learning efficient anomaly detectors from k-nn graphs. In *Artificial Intelligence and Statistics*, pages 790–799, 2015.

H. Rootzén, J. Segers, and J. L. Wadsworth. Multivariate peaks over thresholds models. *Extremes*, 21(1):1–31, 2016.

H. Rootzén, J. Segers, and J. Wadsworth. Mutlivariate peaks over threshold models. *Extremes*, 21:115–145, 2018.

R. E. Serfling. Methods for current statistical analysis of excess pneumonia-influenza deaths. *Public health reports*, 78(6):494, 1963.

L. Simonsen, M. Clarke, L. Schonberger, N. Arden, N. Cox, and K. Fukuda. Pandemic versus epidemic influenza mortality: a pattern of changing age distribution. *Journal of Infectious Diseases*, 178(1):53–60, 1998.

E. W. Steyerberg, A. J. Vickers, N. R. Cook, T. Gerds, M. Gonen, N. Obuchowski, M. J. Pencina, and M. W. Kattan. Assessing the performance of prediction models: A framework for traditional and novelmeasures. *Epidemiology*, 21:128–138, 2010.

A. Thomas, S. Clémençon, A. Gramfort, and A. Sabourin. Anomaly detection in extreme regions via empirical MV-sets on the sphere. In *AISTATS*, pages 1011–1019, 2017.

M. Thomas, M. Lemaitre, M. Wilson, C. Viboud, Y. Yordanov, H. Wackernagel, and F. Carrat. Applications of extreme value theory in public health. *PLoS ONE*, 11(7), 2016.

C. Viboud, P.-Y. Boëlle, K. Pakdaman, F. Carrat, A.-J. Valleron, and A. Flahault. Influenza epidemics in the United states, France, and Australia, 1972—1997. *BMC Infectious Diseases*, 10, 2004.